First results to evaluate losses and gains in solar radiation collected by solar tower plants

Cite as: AIP Conference Proceedings **2126**, 190012 (2019); https://doi.org/10.1063/1.5117709
Published Online: 26 July 2019

Mustapha Moulana, Thierry Elias, Céline Cornet, and Didier Ramon

First Results to Evaluate Losses and Gains in Solar Radiation Collected by Solar Tower Plants

Mustapha Moulana[1, 2, a)], Thierry Elias[1], Céline Cornet[2], Didier Ramon[1]

[1]Hygeos, Euratechnologies, 165 Avenue de Bretagne, 59000 Lille, France.
[2]*Univ. Lille, CNRS, UMR 8518 – LOA – Laboratoire d'optique atmosphérique, F-59000, France.*

[a)]Corresponding author: mm@hygeos.com

Abstract. Accurate computation of Solar Tower Plants (STPs) accounting for the atmospheric scattering gain and loss is nowadays possible with new technologies (computation performance growth). Radiative Transfer (RT) codes can be improved to perform directly and complete optical simulation of incident solar radiation in STPs. In this work, the RT SMART-G code, enabling fast computation thanks to GPU technology, have been improved to enables interactions between solar radiation and objects. Considering all the possible optical paths, a classification of the solar beams received by STPs is presented. The preliminary results obtained with a simplified STP, show that the gains due to atmospheric contribution at STPs receiver with an average horizontal heliostat-receiver distance from 200 to 900 meters is between 0.7% to more than 5%, depending on the aerosol optical thickness. The studied system is currently a simplified STP of maximum eight heliostats, but it is a promising way for other studies with more realistic STP and different illumination conditions.

INTRODUCTION

Solar **T**ower **P**lants (STPs) efficiency prediction or validation needs an accurate solar resource assessment, which is a difficult task as large variations of atmospheric parameters lead to a large variation of the solar resource. STPs simulation by considering all these variabilities requires huge performance in computation. Studies concerning the estimation of the solar resource is thus generally separated in two parts. The first part consists to get the solar radiation incoming at heliostats, using based-ground observations or **R**adiative **T**ransfer (RT) codes to estimate the **D**irect **N**ormal **I**rradiance (DNI). The second part, using the DNI as an input parameter, consists to simulate the propagation of the solar radiation in the slant path between heliostats and the receiver using **O**ptical **S**imulations (OS) codes as DELSOL3, MIRVAL, HELIOS [1, 2, 3], or more recently SOLFAST, SolTRACE, Tonatiuh [4, 5, 6]. These codes have limitations, DELSOL3 for example, consider the atmospheric attenuation as only dependent on the slant path distance [8]. Whereas several studies have recently proven that the atmospheric attenuation efficiency (called the Slant Path Transmittance) is also greatly dependent on the atmospheric parameters [8, 9]. Currently, to our knowledge, [8, 9] give the most accurate estimates of the atmospheric attenuation, but scattered beams are only considered as a loss, while it may represent a potential gain. Blanc *et al.* [10] mention these gains in the circumsolar region, corresponding to the forward scattering of sunlight by cloud or aerosol particles, but only for the DNI estimation. Some OS codes use the model of Buie *et Monger* [11] to approximate, in the slant path, the distribution of scattered beams. However, this model gives only the approximation of the distribution and not on the gains contribution. To consider the contribution of gains and provide better estimates of the solar resource, the propagation of solar radiation can be simulated from the sun to directly the receiver by using RT codes. The main limitation of such simulation is the huge computational time. However, with the exponential increase of **G**raphic **P**ower **U**nit (GPU) performance, such an ambition is now possible. In addition of considering the gain contribution, this direct simulation of the collected solar resource offers the advantage of conserving the same atmospheric input data (in situ or/and satellite data) and uncertainties as for the RT codes estimates of DNI. There is for example no addition of uncertainties of independent studies for the atmospheric loss estimates. The interest of such a model is shown in this paper. We use the parallelized

SolarPACES 2018
AIP Conf. Proc. 2126, 190012-1–190012-8; https://doi.org/10.1063/1.5117709
Published by AIP Publishing. 978-0-7354-1866-0/$30.00

RT SMART-G code enabling the estimates of the incident intensity also directly at STPs receiver. The optical losses [12] are automatically considered in SMART-G and we focus on the gain contribution at the receiver. The simplified system used (STP of maximum eight heliostats) enables to have an order of gain contribution from small SPT to larger SPTs, with an average horizontal heliostat-receiver distance D_{hr} respectively from 200 to 900 meters. The atmosphere is defined from observation measurements.

In the method section, we firstly present the radiative transfer model used to conducts the studies, afterwards the classification used for the receiver incident intensity, then the definition of optical losses and gains, and finally the description of the performed simulations with modeling, technical parameters, location parameters, etc.

METHOD

The SMART-G Simulation Tool

Speed-Up **M**onte-Carlo **A**dvanced **R**adiative **T**ransfer code with **G**PU (SMART-G) [13] is the chosen tool to perform this study, this is a polarized Monte Carlo RT code. It enables to simulate the propagation of the light in both the atmosphere and the ocean. The solar beams can be absorbed and scattered by the atmosphere components as molecules, aerosols and droplets, and also reflected by the ground. SMART-G has been improved to allow the interactions of solar beams with objects (i.e. heliostats, receiver...). The information of each solar beam from start to end of their travel are available, allowing the estimation of losses and gains of the incident intensity at the receiver.

Solar Beams Incident at the Receiver Classified in Several Categories (Theoretical Background)

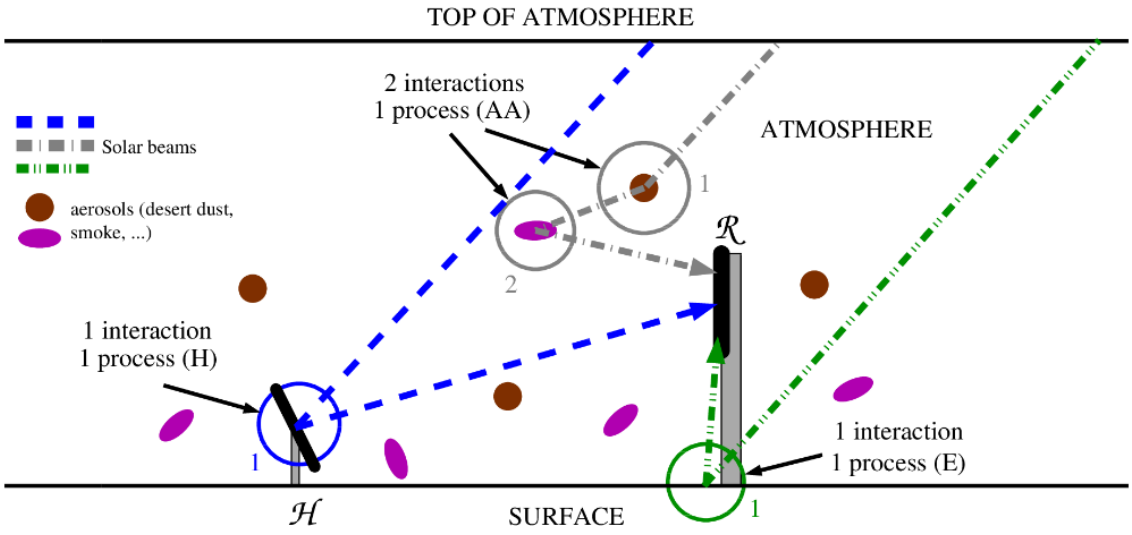

FIGURE 1. Schematic of three beams reaching the receiver R from three different paths. One path where the beam (blue dashed line) gets one interaction from the process of heliostats reflection (reflected by the heliostat H), the second beam (green two dot-dashed line) gets also one interaction but from the process of environment reflection (here the ground), and the last beam (grey dot-dashed line) get two interactions, both from the process of atmospheric scattering.

Figure 1 gives a schematic view of three solar beams incoming at the receiver from three radiative processes responsible to a trajectory modification. The first process is the Atmospheric scattering (A), the second process the reflection by a Heliostat (H) and the last process the reflection by an element of the Environment (E) as the ground, building, vegetation, etc. As shown in Fig.1, the solar beams incident at the receiver can be separated in several pieces. In this study we have chosen to divide them in eight categories following the three radiative processes outlined above (see Tab.1). The abbreviation AA in Tab.1, for instance, means two interactions with only the process of Atmospheric scattering as shown in Fig.1 with the grey dot-dashed line. The abbreviation D (for direct) refers to the case where the solar beam reaches the receiver without any processes.

TABLE 1. Solar beams from all the possible optical paths, classified with three radiative processes in eight categories. Only possible paths from one to three interactions are given, but the classification is valid for any number of interactions. The category colors are helpful for the Fig.1, 4 and 5.

	Number of Processes	Which Process(es)	Possible Paths from 1 to 3 Interactions
Cat.1	0	without any processes	D
Cat.2	1	Heliostat reflection (H)	H, HH, HHH
Cat.3	1	Environment reflection (E)	E, EE, EEE
Cat.4	1	Atmosphere scattering (A)	A, AA, AAA
Cat.5	2	H and A	HA, AH, AAH, AHA, AHH, HHA, HAH, HAA
Cat.6	2	H and E	HE, EH, HHE, HEH, HEE, EEH, EHE, EHH
Cat.7	2	E and A	EA, AE, AAE, AEA, AEE, EEA, EAE, EAA
Cat.8	3	H and E and A	AHE, AEH, HAE, HEA, EAH, EHA

Optical Losses & Gains

Heliostat field performance of STPs is defined by the optical efficiency, noted η_{opt}, following this equation [14]:

$$\eta_{opt} = \frac{P_{field}}{A_{field} \cdot I_s} \quad (1)$$

In Eq.1, A_{field} corresponds to the total of the heliostat field surface (m^2), I_s the DNI (W/m^2) and P_{field} the power intercepted by the receiver (W). This efficiency depends on different types of optical losses defined by Li *et al* [12] : 1) the cosine effect, referring to the loss due to the tilt angle between the heliostat surface normal compared to the incident beam, 2) the spillage loss, representing the beams missing the receiver due to the heliostat roughness surface, heliostat misalignment and small receiver aperture, 3) the attenuation loss which is the atmospheric extinction loss between the heliostat and the receiver, 4) the reflection loss which concerns the heliostat reflectivity loss, affected for instance by the heliostat soiling, 5) the shadows loss which is due the shadows created by another heliostat, the tower, the receiver, etc. and 6) the blocking loss which designates the loss after heliostats reflection due to an obstacle as a second heliostat.

According to other authors, we define P_{field} (in Eq.1) as the power intercepted by the receiver of solar beams incident with only the process of heliostat reflection (corresponding to Cat.2 in Tab.1). That is why the power of the other incident solar beams (corresponding to solar beams from all the categories except Cat.2) are considered as gains.

Simulations Description

TABLE 2. Receiver and heliostat characteristics

Heliostat	Reflectivity []	0.88
	Width [m]	12.84
	Height [m]	9.45
	Pillar Height [m]	5.17
Receiver	Height of receiver middle [m]	106.5
	Inclination angle [°]	11.5
	Width [m]	14
	Height [m]	12

In this study, we are interested in the gain contribution and since a part of gains comes from the atmospheric scattering, an area where solar radiation can be highly scattered is preferred. We have chosen to take an atmospheric profile corresponding to the Noor III STP location, where there is a huge variation of desert aerosols. The AFGL midlatitude summer profile [15] has been chosen and proportionally modified to allow a surface pressure of 877 hPa (altitude of Noor III), water vapor values were also modified to fill 1.2 g/cm² (AERONET average observation at Ouarzazate summer [16]). A desert spheroid aerosols OPAC profile has been chosen [17]. According to the Noor III

location measurements, the average **A**erosol **O**ptical **T**hickness (AOT) in summer is usually 0.4 and can also reach a value of 1 (daily resolution) [16]. For the simulations the choice of AOT values are then: 0.25, 0.5, 0.75 and 1.

We start in this paper with preliminary computations of simple systems composed of a receiver and a maximum of eight heliostats (variation of the number of heliostats: 1, 2, 4 and 8). Because of a lack of information for Noor III and for more simplicity, the receiver and heliostats modeling has been inspired by the PS10 STP [18, 19]. For instance, the PS10 receiver is inside a cavity which can be assimilated by a simple rectangular form. The chosen parameters are summarized in Tab.2.

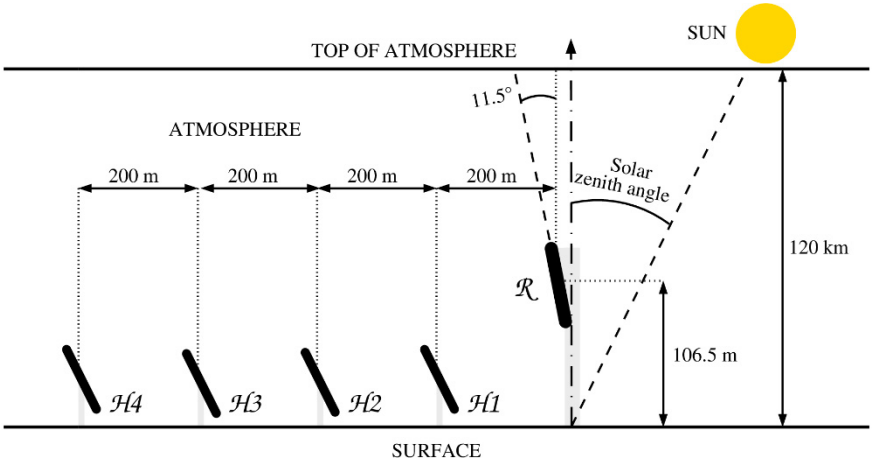

FIGURE 2. Schematic description of the position of the receiver R and the heliostats H1, H2, H3 and H4.

Figure 2 shows a schematic of our simulations (case with 4 heliostats). The increase of the number of heliostats is done along a straight line (North-South). The first heliostat is at 200 meters (horizontally) from the receiver, and each added heliostat is further than the previous one of 200 meters. This gap allows to avoid as much as possible the shadows and blocking losses. The maximum horizontal heliostat-receiver distance is 1.6 kilometers (case for simulations with 8 heliostats), this is in average the maximum horizontal receiver-heliostat distance of huge STPs as Noor III and Crescent Dunes. The sun is behind the receiver (the receiver faces North and is in shadows) and the zenith angle is equal to 14.3°, corresponding to the noon position at Ouarzazate, Morocco.

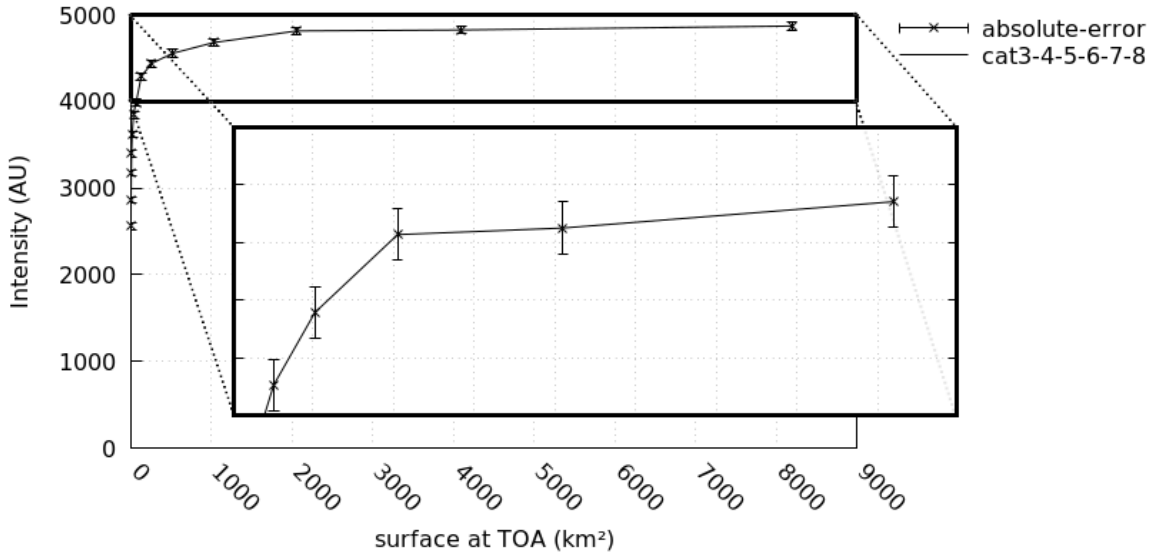

FIGURE 3. Sum of receiver incident intensities (Arbitrary Unit) of solar beams from Cat.3, 4, 5, 6, 7 and 8 (vertical axis) in function of the size of the square zone at TOA (horizontal axis).

Figure 3 shows the intensity variation of all the solar beams incident at the receiver except the direct solar beams and the solar beams incident with only the process of heliostat reflection (i.e. solar beams from all the categories except from Cat.1 and 2 in Tab.1) in function of the size of the surface where they are distributed at **T**op **O**f **A**tmosphere (TOA). A square surface at TOA is used as the input of solar beams to consider the influence of solar beams from Cat.3, 4, 5, 6 and 7. The horizontal position of this square zone depends of the sun zenith angle and of the receiver position. Such as the center of the surface produced by the direct solar beams reaching the ground is coincident with the horizontal position of the receiver. More the square surface at TOA is large more the atmosphere influence is accurately considered, but also a larger number of solar beams is needed. Then to define an optimum minimal size, we performed different simulations with one heliostat at 200 meters horizontally from the receiver by varying the size of the square surface from 1 km² to almost 9000 km². For a size of approximately 2000 km² a stabilization is observed in Fig.3. The square surface size is thus set to 45 x 45 km².

By accounting the variation of AOT values and the number of heliostats, there are sixteen simulations. The simulations are performed with 200 billion of beams from TOA in a plan-parallel atmosphere for monochromatic radiation at a wavelength of 550 nm, which is usually taken as reference [9]. The ground is considered as a plane Lambertian surface with an albedo of 0.25, this is approximately the spectral average surface albedo of a stone-desert surface in many parts of the Ouarzazate basin [20]. The attenuation, the cosine and reflectivity losses are taken into account, the shadow and blocking losses are supposed to be negligible and there is an absence of surface roughness at the heliostats.

RESULTS AND DISCUSSION

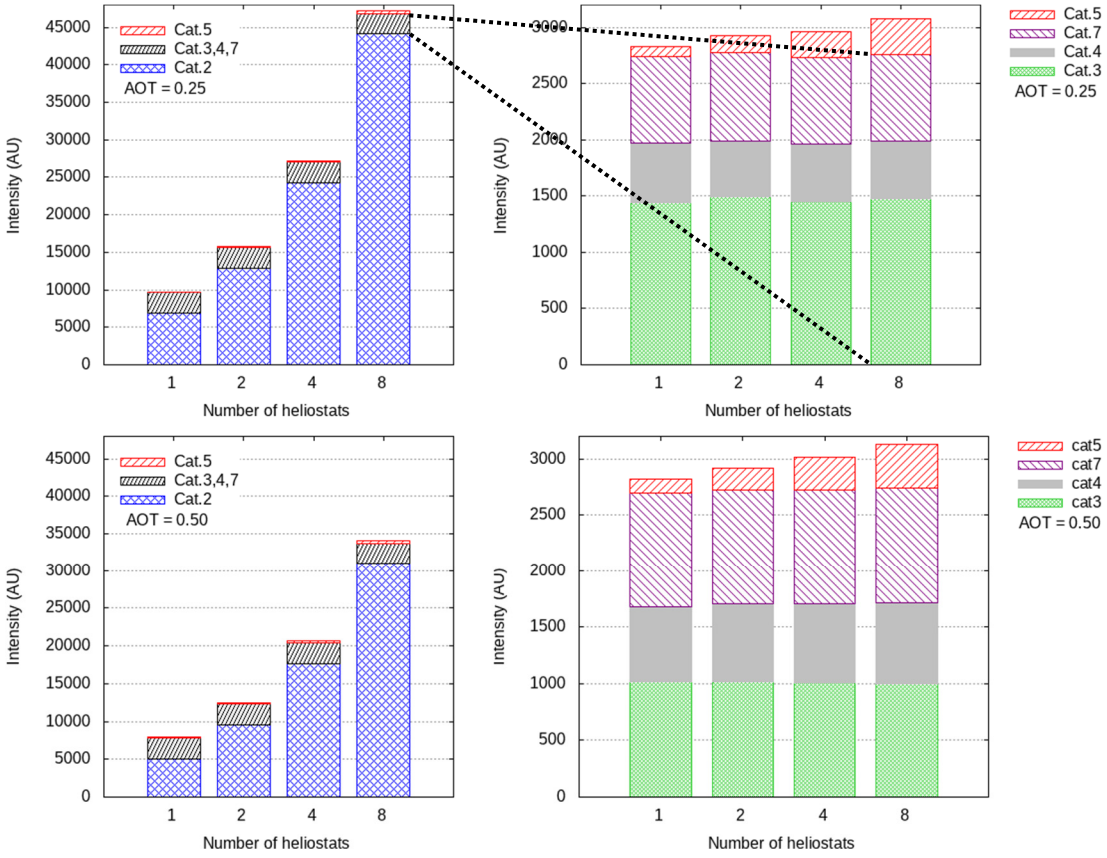

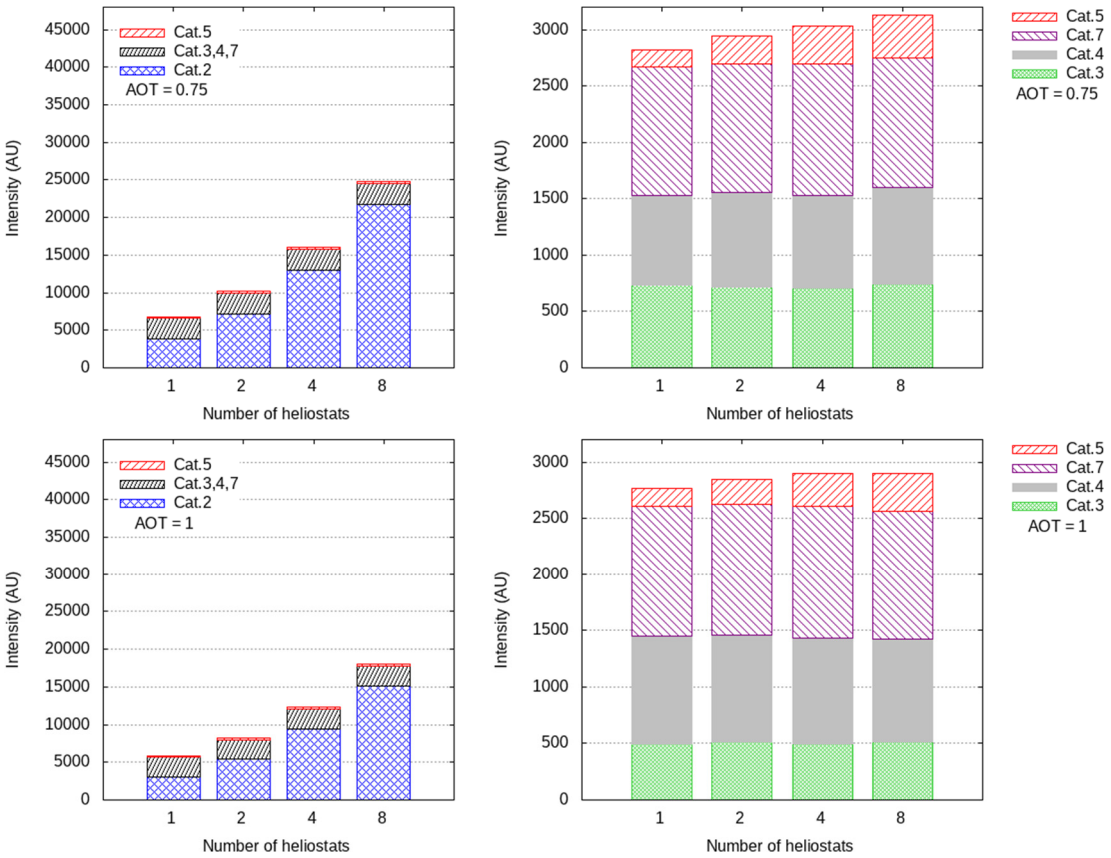

FIGURE 4. Receiver incident intensities (Arbitrary Unit) of solar beams from Cat.2, 3, 4, 5 and 7 for AOT of 0.25, 0.5, 0.75 and 1 in the first column. Intensities of solar beams from all the same categories except Cat.2 in the second column.

Figure 4 shows the decomposition of the total incident intensity at the receiver following the classification of Tab.1. As the sun is behind the receiver, the direct solar beams coming at the receiver without any radiative processes (Cat.1) is always null. As there is no heliostat surface roughness, as the ground is a plane surface and as heliostats are oriented to reflect all the direct beams to the receiver, the case where solar beams reach the receiver with only the two processes of heliostat reflection and environment reflection (Cat.6) is not possible. The computed intensity of solar beams reaching the receiver through the three radiative processes (Cat.8) is for all our simulations very close to zero. Then the solar beams from Cat.1, 6 and 8 are not represented.

Figure 4 (first column) shows the intensities of solar beams reaching the receiver with only the process of heliostat reflection (Cat.2), with only the two processes of heliostat reflection and atmospheric scattering (Cat.5), and without the heliostat reflection process (sum of Cat.3, 4 and 7). Figure 4 (second column) gives a zoom of all these intensities except from solar beams incident with only the process of heliostat reflection (Cat.2).

In Fig. 4, the increase of the number of heliostats (same behavior for the four AOT) leads logically to an increase of the intensity from solar beams reaching the receiver with at least a process of heliostat reflection (Cat.2 and 5). For solar beams with at least a process of environment scattering (Cat.3 and 7), the increase of the number of heliostats create a diminution of the ground surface, so we excepted a decrease of surface reflection and hence of intensity. But, the number of heliostats for these simulations is too small. The solar beams with only the atmospheric scattering process (Cat.4), is as excepted independent on the number of heliostats. The increase of AOT (conducting to a scatter probability growth) leads as expected to an increase of the intensity from solar beams incident with at least an atmospheric scattering process (Cat.4 and 7), and to a decline of the intensity from solar beams incident at the receiver without the atmospheric scattering process (Cat.2 and 3).

The aim is to assess the contribution of solar beams intensity of each category collected by a realistic STP. As previously commented, the intensities of solar beams from Cat.3, 4 and 7 do not vary or must decrease with the number of heliostats, and then in a realistic STP their contributions will become negligible. The only remaining contributions are from solar beams classified by Cat.2 and 5. In Eq.1 we have previously defined P_{field} (reference for losses and

gains) as the power of solar beams incident with only the process of heliostat reflection (Cat.2). Figure 5 shows then the gain contribution of Cat.5 intensity, which represents combination of atmospheric scattering and heliostat reflection processes, compared to Cat.2 intensity. Figure 5 shows that relatively to Cat.2, Cat.5 contribution is increasing by AOT (due to a large decrease of Cat.2). However, this contribution decreases by increasing the D_{hr} value. This is logical because there is no loss due to beams missing the receiver from Cat2 (no consideration of heliostat surface roughness). For the solar beams of Cat.5 (incorporating the forward scattered beams) there are losses because the aperture of solar beams reaching the receiver increases with the D_{hr}.

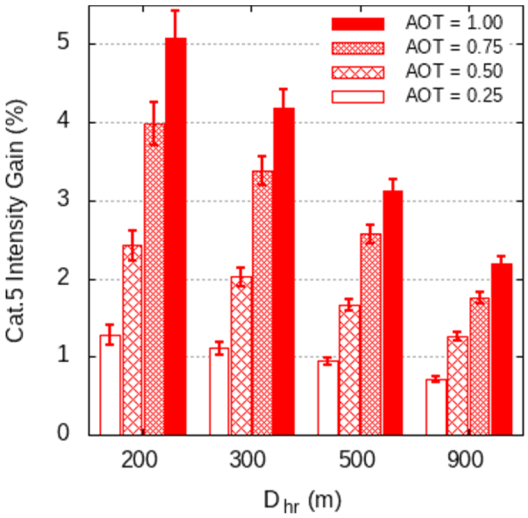

FIGURE 5. Percentage of gain from Cat.5 intensity relatively to Cat.2 intensity (reference for gains and losses) at the receiver, in function of AOT and the horizontal average heliostat-receiver distance (D_{hr}).

CONCLUSION

This study presents preliminary results towards the accurate computation of the solar radiation incident intensity at the receiver of a STP. Several simulations have been performed to study the sensibility of three parameters, the number of heliostats, the D_{hr} and AOT. Currently, the STP used for the simulations is composed of maximum eight heliostats with no surface roughness, and with an environment comprising a desert-stone plane ground. Following these conditions, the intensities of solar beams incident at the receiver with only the two processes of heliostat reflection and environment (here the ground) reflection, and with all the three radiative processes at the same time are equal or very close to zero (solar beams from Cat.6 and 8 in Tab.1). The only contributions, which is increasing with the number of heliostats, correspond to intensities from solar beams incident with only the heliostat reflection process and to solar beams incident with the combination of the two processes of atmospheric scattering and heliostat reflection (respectively solar beams from Cat.2 and 5 in Tab.1). The main contribution, used as reference for losses and gains, is as expected the intensity of solar beams incident with the only process of heliostat reflection (Cat.2). The other intensities of solar beams incident with only the process of environment reflection, with only the process of atmospheric scattering and with only the two processes of environment reflection and atmospheric scattering (solar beams from Cat.3, 4 and 7 in Tab.1) are as predicted independent on the number of heliostats. They will then be negligible for STP with hundreds of heliostats. For huge STP, with a D_{hr} of 900 meters, the gain contribution is then equal to 0.71% for an AOT of 0.25 and can reach 2.2% for an AOT of 1. For a small STP, with a D_{hr} of 200 meters, this gain contribution is equal to 1.28% for an AOT of 0.25 but can reach 5.08% for an AOT of 1. We observe at the receiver the same order of gain contribution than [10] at heliostats with DNI. The results are expected to be different for other configurations. For example, a higher receiver as the Crescent Dunes STP receiver, will certainly increase the gain contribution from Cat.5 because of a larger receiver aperture. The gains may also increase for larger zenith angles. In addition, a lot of parameters have been neglected, for instance the blocking and shadows losses. The consideration of these parameters can lead to different conclusions and then deserve to be analyzed. Additionally, an implementation of a disk sun source with consideration of the sun solid angle for a more accurate sunshape as Reinhard [21] is planned in SMART-G. Once all these improvements would have been implemented in SMART-G, simulations for a complete STP for the whole solar spectral range will be realized to obtain more realistic computed powers.

REFERENCES

1. B. L. Kistler, "A user's manual for DELSOL3: a computer code for calculating the optical performance and optimal system design for solar thermal central receiver plants," Sandia Labs., SAND86-8018 (1986).
2. P. L. Leary and J. D. Hankins, "User's guide for MIRVAL: a computer code for comparing designs of heliostat-receiver optics for central receiver solar power plants," Sandia Labs., CA (USA). SAND-77-8280 (1979)
3. F. Biggs and C.N. Vittitoe, "HELIOS: A computational model for solar concentrators," Sandia Labs., Albuquerque, NM (USA), SAND-77-0642C, CONF-770630-2 (1977).
4. J.P Roccia, B. Piaud, C. Coustet, C. Caliot, E. Guillot, G. Flamant, G. and J. Delatorre, "SOLFAST, a Ray-Tracing Monte-Carlo software for solar concentrating facilities," in Journal of Physics, Conference Series, IOP Publishing, **369(1)**, 012029 (2012).
5. T. Wendelin, "SolTRACE: a new optical modeling tool for concentrating solar optics," in ASME 2003 International Solar Energy Conference, American Society of Mechanical Engineers, 253-260 (2003).
6. M. J. Blanco, "Tonatiuh: An object oriented, distributed computing, Monte-Carlo ray tracer for the design and simulation of solar concentrating systems," (2016).
7. F. Rinaldi, M. Binotti, A. Giostri and G. Manzolini, "Comparison of linear and point focus collectors in solar power plants", Energy Procedia, **49**, 1491-1500 (2014).
8. N. Hanrieder, S. Wilbert, R. Pitz-Paal, C. Emde, J. Gasteiger, B. Mayer and J. Polo, "Atmospheric extinction in solar tower plants: absorption and broadband correction for MOR measurements," Atmospheric Measurement Techniques, **(8)**, 3467-3480 (2015).
9. T. Elias, D. Ramon, L. Dubus, C. Bourdil, E. Cuevas-Agulló, T. Zaidouni and P. Formenti, "Aerosols attenuating the solar radiation collected by solar tower plants: the horizontal pathway at surface level," in AIP Conference Proceedings, **1734(1)**, 150004 (2016).
10. P. Blanc, B. Espinar, N. Geuder, C. Gueymard, R. Meyer, R. Pitz-Paal, B. Reinhardt, D. Renné, M. Sengupta, L. Wald and S. Wilbert, "Direct normal irradiance related definitions and applications: The circumsolar issue," Solar Energy, **110**, 561-577 (2014).
11. D. Buie and A. G. Monger, "The effect of circumsolar radiation on a solar concentrating system," Solar Energy, **76(1-3)**, 181-185 (2004).
12. L. Li, J. Coventry, R. Bader, J. Pye and W. Lipiński, "Optics of solar central receiver systems: a review," Optics Express, **24(14)**, A985-A1007 (2016).
13. D. Ramon, F. Steinmetz, D. Jolivet, M. Compiègne and R. Frouin, "Modeling polarized radiative transfer in the ocean-atmosphere system with the GPU-accelerated SMART-G Monte Carlo code," in Journal of Quantitative Spectroscopy and Radiative Transfer, **222**, 89-107 (2019).
14. A. Danielli, Y. Yatir and O. Mor, "Improving the optical efficiency of a concentrated solar power field using a concatenated micro-tower configuration". Solar Energy, **85(5)**, 931-937 (2011).
15. G. P. Anderson, S. A. Clough, F. X. Kneizys, J. H. Chetwynd and E. P. Shettle "AFGL atmospheric constituent profiles (0.120 km)," AIR FORCE GEOPHYSICS LAB HANSCOM AFB MA, AFGL-TR-86-0110 (1986).
16. T. Elias, D. Ramon, M. Moulana and J-F. Brau, "Sensitivity of the solar resource in solar tower plants to aerosols and water vapor," AIP Conference Proceedings (forthcoming).
17. M. Hess, P. Koepke and I. Schult, I, "Optical properties of aerosols and clouds: The software package OPAC," Bulletin of the American meteorological society **79(5)**, 831-844 (1998).
18. R. Osuna, R. Olavarrıa, R. Morillo, M. Sánchez, F. Cantero, V. Fernández-Quero, P. Robles, T. L. del Cerro, A. Esteban, F. Cerón, J. Talegón, M. Romero, F. Téllez, M. J. Marcos, D. Martínez, A. Valverde, R. Monterreal, R. Pitz-Paal, G. Brakmann, V. Ruiz, M. Silva and P. Menna, "PS10, Construction of a 11MW solar thermal tower plant in Seville, Spain," in SolarPACES Conference (Seville, Spain, 2006), pp. 20-23.
19. F. Eddhibi, M. B. Amara, M. Balghouthi and A. Guizani, "Optical study of solar tower power plants," in Journal of Physics, IOP Publishing, Conference Series **596(1)**, 012018 (2015).
20. E. Bierwirth, M. Wendisch, A. Ehrlich, B. Heese, M. Tesche, D. Althausen, A. Schladitz, D. MüLLER, S. Otto, T. Trautmann, T. Dinter, W. V. Hoyningen-HUENE and R. Kahn, "Spectral surface albedo over Morocco and its impact on radiative forcing of Saharan dust," Chemical and Physical Meteorology **61(1)**, 252-269 (2009).
21. B. Reinhardt, R. Buras, L. Bugliaro, S. Wilbert and B. Mayer, "Determination of circumsolar radiation from Meteosat Second Generation," Atmos. Meas. Tech. **7**, 823-838 (2014).